[PROC. OF JSCE Structural Eng./Earthquake Eng. Vol. 1, No. 2 October 1984]

STUDY ON COMPLEXITY OF LARGE EARTHQUAKES

By Masahiro IIDA and Motohiko HAKUNO***

We clarify the complexity of large earthquakes by considering the ground motions of short-period range. First, an approach is applied to three large earthquakes in Japan by which the accelerograms of a large earthquake are synthesized from the accelerograms of a small one. As a result, it is shown that this approach can be applicable to some degree, but a larger earthquake is more complicated. Next, an inversion method applicable to the analysis of the source rupture process corresponding to short-period range is proposed and is applied to the 1968 Tokachi-oki, Japan, earthquake. It is inferred from the obtained results that this earthquake has a complicated source rupture process and has source directivity even in short-period range. It is thought that this inversion method is exceedingly effective.

1. INTRODUCTION

We[1] produced accelerograms, applying the approach suggested by Hartzell[2] to short-period range. The approach is to synthesize the record of a large earthquake by using the record of a small earthquake as Green's function. The results were relatively good and this approach had bright prospects. This approach has the advantage that the effects of source and earth response are included in the modeling process, since both the large earthquake and the small one occurred in the same source region and were recorded at the same observation station. Therefore, the meaning of the method is physically proper and there is no need of a lot of calculations.

The major objective of this study is to make clear the complexity of large earthquakes by considering the ground motions of short-period range. First, a revised approach[1] is applied to three large earthquakes and the validity of the method is examinied. Next, the inversion method, which clarifies a source rupture process using some seismograms, is developed and is applied to the earthquake (or the seismogram) which can not be explained well by the revised approach.

2. REVISED APPROACH

(1) Objective

Though the approach was effective to some degree[1], we need to examine the validity of the approach. After improving it, we apply the revised approach to three large earthquakes, namely, the 1978 Miyagiken-oki, Japan, earthquake (the magnitude by the Japan Meteorological Agency, M_J, is 7.4 and the corresponding observation station is Miyako), the 1973 Nemurohanto-oki, Japan, earthquake (7.4,

* Member of JSCE M. Eng., Res. Assoc., Earthquake Research Institute, Univ. of Tokyo (Bunkyo-ku, Tokyo)
** Member of JSCE Dr. Eng., Professor, Earthquake Research Institute, Univ. of Tokyo (Bunkyo-ku, Tokyo)

Kushiro) and the 1968 Tokachi-oki, Japan, earthquake (7.9, Hachinohe). They are all interpreted as the typical shallow earthquakes of a low-angle thrust type which occur off the Pacific coast of Japan[3)~5)]. In this study, only strong motion accelerograms are used. The correction of instrumental response of these records has already been done. In this (the second) chapter, two horizontal (E-W and N-S) components are employed.

(2) Method

Although the method was shown in the previous paper[1)], there are four improvements in this simulation. We summarize the revised method briefly while we point out the improvements. It is assumed that a large earthquake can be represented as the superposition of small earthquakes and that elements are broken one after another as the rupture propagates along a fault. It is assumed that the synthesized wave is written in the following equation:

$$F(t)=\sum_{e=1}^{X}\alpha_e \cdot g_e(t) * h_e(t) * E_e\left(t-\frac{s_e}{v_e}-\frac{r_e}{u_e}\right) \quad (1)$$

where X is the total number of elements, E is the observed record of a small earthquake (the elemental wavelet), s is the distance between the starting point of rupture and an element, v is the rupture velocity of a fault, r is the distance between an element and the observation station, u is wave velocity, α is a coefficient for the correction of radiation pattern, g is a function for the correction of hypocentral distance, h is a function for the correction of the magnitude of a shock, $*$ is convolution operator, t is the time and subscript e indicates the e-th element. A Eq. (1) are further explained in each part.

a) Size and Location of Fault Zone

The size and location of a fault zone is determined on the basis of aftershock distribution, a tunami source area and the result of analysis of long-period surface-waves.

b) Total Number of Elements

The total number of elements, X, is taken equal to the ratio of the seismic moment, M_0, for a large earthquake to that for a small one. The seismic moment is calculated from M_J, using the regression equation[1)]:

$$\log_{10} M_0(N\cdot m)=1.60\,M_J+8.4 \quad (2)$$

The seismic moment is distributed uniformly over the fault plane. We consider that the amount of short-period components generated from per unit area and unit dislocation is the same for large and small earthquakes, and assume the following relation:

$$h_e=\text{const.}=1 \quad (3)$$

In order to interpret: results simply, the synthesis is done from the record of only a single small earthquake:

$$E_e(t)=E(t) \quad (4)$$

We select the small earthquake that can be regarded as a point source (an event in the far-field) and the amplitude of which is recorded with enough accuracy (the 1-st improvement).

Table 1 Hypocentral parameters of three large earthquakes and corresponding small ones.

	Miyagiken		Nemurohanto		Tokachi	
	Large	Small	Large	Small	Large	Small
Origine date	June 12, 1978	February 20, 1978	June 17, 1973	May 11, 1972	May 16, 1968	March 20, 1972
Latitude (degree)	38.15 N	38.75 N	42.97 N	42.60 N	40.68 N	40.85 N
Longitude (degree)	142.17 E	142.20 E	145.95 E	144.90 E	143.58 E	142.00 E
Depth (km)	40	50	40	60	0	80
Magnitude (M_J)	7.4	6.7	7.4	5.8	7.9	6.5

c) Rupture Propagation

We model the irregularity of rupture propagation in terms of circular wave front concentric at the starting point of rupture, in order to prevent the strong dependence of the frequency components upon the size of an element (the magnitude of a selected small earthquake) and to disperse the phases of elemental wavelets. After deviding the fault plane into 8 zones, the rupture front, which spreads at the variable speed of normal distribution, is made by a Monte-Carlo search, independently in each zone :

$$v_e = v_\mu(m_\mu,\ \sigma_\mu)\ \ (\mu=1\sim8) \cdots\cdots (5)$$

$$\sigma_\mu = 0.5\, m_\mu = \text{const.}\ \ (\mu=1\sim8) \cdots\cdots (6)$$

where m_μ is an average and σ_μ is a standard deviation. The commencement of the main-fault propagation is looked upon as the starting point of rupture in this simulation (the 2-nd improvement). In addition, since the rupture velocity evaluated from long-period surface-waves is inaccurate, we change this parameter to obtain the optimum value (the 3-rd improvement).

d) Wave Propagation

This synthesis is applied to the S-waves which form the main parts of strong ground accelerograms. For simplification, it is assumed that the wave velocity is constant :

$$u_e = \text{const.} = V_s\,(S\text{-wave velocity}) \cdots\cdots (7)$$

With regard to a_e, radiation pattern is disregarded :

$$a_e = \text{const.} = 1 \cdots\cdots (8)$$

The correction of source direction is done by transforming two horizontal components into the longitudinal and transverse components. With regard to g_e, the amplitude reduction in proportion to $1/r$ and the internal damping are taken into account (the 4-th improvment). When we define the corrected elemental wavelet as E'_e, g_e are represented in the following Eqs. (9)-(12) :

$$E'_e(t) = g_e(t) * E(t) \cdots\cdots (9)$$

$$E'_e(t) = \int_{-\infty}^{\infty} \exp(D_e f + I\,2\pi f t)\cdot W_e(f)\, df \cdots\cdots (10)$$

$$W_e(t) = \int_{-\infty}^{\infty} E(t)\cdot\frac{r}{r_e}\cdot\exp(-I2\pi f t)\, dt \cdots\cdots (11)$$

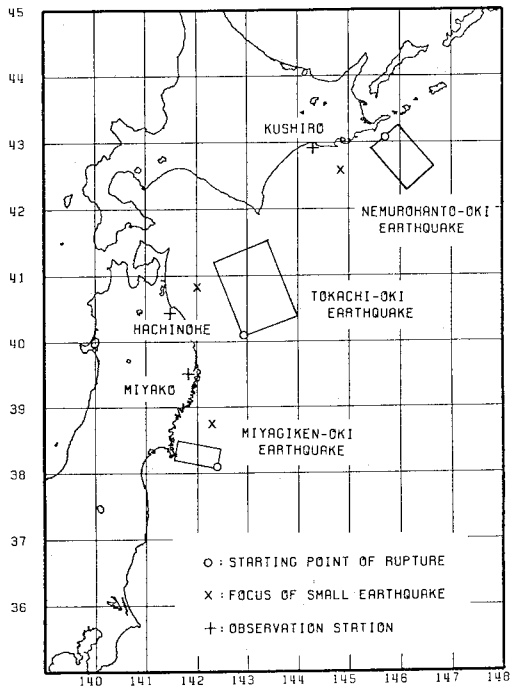

Fig. 1 The fault zones and observation stations for three earthquakes.

Table 2 The parameters of three earthuakes used for the simulations.

		Miyagiken	Nemurohanto	Tokachi
Fault length (km)		30	60	150
Fault width (km)		80	100	100
Central point of fault	Latitude (degree)	38.33 N	42.75 N	*40.83 N
	Longitude (degree)	142.00 E	146.00 E	*143.17 E
	Depth (km)	35	33	*33
Dip direction (degree)		N 10 E	N 40 W	*S 66 W
Dip angle (degree)		20	27	*20
Magnitude of large event		7.4	7.4	7.9
Magnitude of small event		6.7	5.8	6.5
Starting point of rupture		Southeastern end	Center of northern side	Southwestern end
Rupture velocity (km/sec) (variable)		2.0, 2.4, 2.8, 3.2, 3.6, 4.0	2.0, 2.4, 2.8, 3.2, 3.6, 4.0	2.0, 2.5, 3.0, 3.5, 4.0
S-wave velocity (km/sec)		4.0	4.0	4.0
S wave quality factor		600	500	500

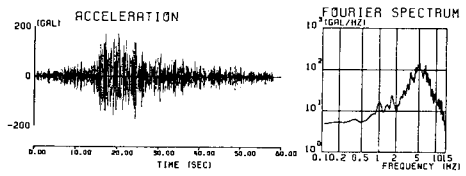

(1) Observed record

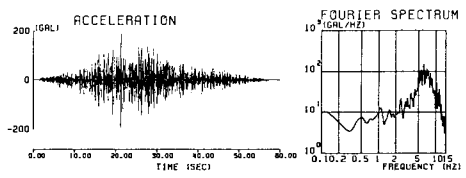

(2) Synthesized wave

Fig. 2 Comparison on the E-W component at Miyako station in the Miyagiken-oki earthquake.

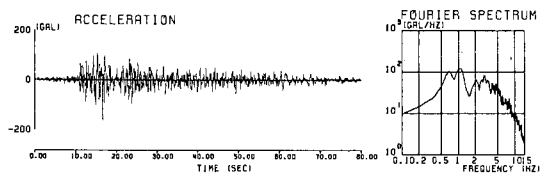

(1) Observed record

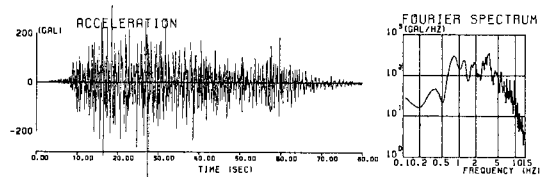

(2) Synthesized wave

Fig. 3 Comparison on the E-W component at Kushiro station in the Nemurohanto-oki earthquake.

$$D_e=\frac{\pi}{V_s}\cdot\left(\frac{r_s}{Q_{ss}}-\frac{r_e}{Q_{se}}\right)\cdots\cdots (12)$$

where Q_{ss} is the S-wave quality factor throgh the wave propagation path of a small earthquake, Q_{se} is the S-wave quality factor through the wave propagation path of each shock, r_s is the hypocentral distance for a small earthquake, f is the frequency and I is the imaginary unit ($I^2=-1$). The following additional condition is given :

$$Q_{se}=Q_{ss}=\text{const.}\cdots\cdots (13)$$

e) Simulation

The large earthquakes and the corresponding small ones used in this simulation are shown in Table 1. The fault zones for three large earthquakes and the observation stations where synthesis is made are illustrated in Fig. 1. The locations of the hypocenters of these small earthquakes are different from those of large earthquakes and we do not examine the faulting mechanism of the small earthquakes. The parameters used for simulation are summarized in Table 2[3)~5)].

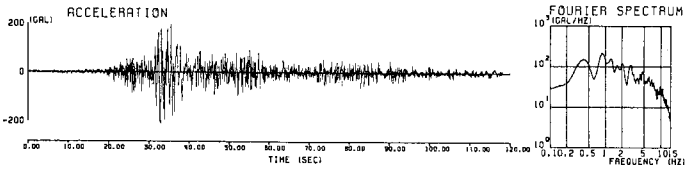

(1) Observed record

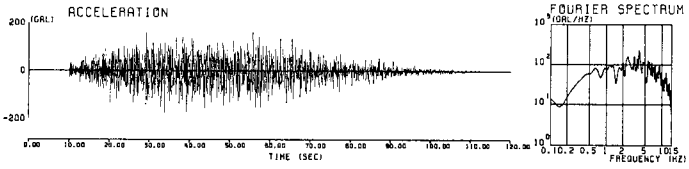

(2) Synthesized wave

Fig. 4 Comparison on E-W component at Hachinohe station in the Tokachi-oki earthquake.

(3) Results

The synthesized waves are compared with the obseved records on the E-W component in Figs. 2, 3 and 4. Although the amplitude of the synthesized wave is twice as large as that of the observed record at Kushiro station, the amplitude of the synthesized waves and that of the obseved records are roughly the same at the other two stations. The optimum value of average rupture velocity, m_μ, is estimated from visual inspection of waveform. Whereas the rupture propagates at the high speed of 3.6 km/sec in the Miyagiken-oki earthquake, the ruptures propagate slowly at the speed of 2.4 km/sec in the Nemurohanto-oki earthquake and 2.5 km/sec in the Tokachi-oki earthquake. In the Miyagiken-oki earthuake, the agreement between the synthesized wave and the observed record is satisfactory in the shape of the envelop of waveform. On the other hand, in the Tokachi-oki earthquake, it is not satisfactory. Besides, the synthesized waves include more short-period components than the observed records in all cases.

(4) Discussion

It has been confirmed that the revised method is successful in all cases to some degree. However, it is impiled that more complicated rupture propagates more slowly as the magnitude of an earthquake grows larger. As it is apparent that the synthesized waveform is not similar to the observed waveform in the Tokachi-oki earthquake, it suggests that the earthquake is far from a simple rupture.

3. INVERSION METHOD

(1) Objective

In the previous chapter, the synthesized wave is not in good agreement with the observed record in the Tokachi-oki earthquake. This fact implies the complexity of this earthquake. Therefore, it is extremely important to clarify a source rupture process corresponding to short-period range. In this chapter, we develop an inversion method and investigate a source rupture process from the accelerograms at several obsevation stations. We apply the inversion method to the 1968 Tokachi-oki, Japan, earthquake, using the accelerograms at four stations.

(2) Recent studies

In this section, the recent prominent studies of inversion are introduced briefly. In 1976, Burdick and Mellman[6] and Langston[7] demonstrated that an inversion approach could be made for a complicated shallow earthquake, by analyzing P-waves and taking the influence of free surface reflection into account. In addition, in 1980, Boatwright[8] carried out a direct deconvolution approach which did not assume a source time function, but employed a free surface operator. In 1982, Kikuchi and Kanamori[9] determined the height and the onset time of constituent source time functions in order of size by a least squares method. An inversion approach can exclude the apparent events which took place before and after an earthquake. Therefore, it is thought that the evaluation from an inversion approach is much more reliable than that from aftershock distribution or surface rupture. However, since no standard method exists, several approaches are made.

On the other hand, in 1970, Trifunac and Brune[10] determined the locations of the events on the basis of the accelerograms at a single station, using the travel time curves of P and S waves. In 1982, Fujino, Hamazaki and Inoue[11] investigated multiple shocks with much the same method, using the many accelerograms at array stations in the near-field. These two studies note the distinct phases of accelerograms. In short-period range, there is no standard criterion for the assumption of a source time function (Green's function for a point source) and for the waveform matching of synthesized waves with observed records. In some cases, the absolute time of accelerogrms is not clear. In addition, short-period waves are affected strongly by the non-linear behavior of soft surface layers. For these reasons, it is very difficult to carry out an inversion approach corresponding to short-period range.

(3) Method

We demonstrate that a source rupture procss is irregular spatiotemporally. This method is composed of two procedures. In the first stage, many synthesized waves are produced by trial and error, and in the second stage, the extent of the agreement of these synthesized waves with an obseved record is estimated. The distinctive feature of this method is to make clear a source rupture process by using the record at the same station of a small earthquake, which took place in the same source region as a large earthquake, as Green's function for a point source, because this makes it possible not to consider the effects of a propagation path and an observation site. The technique is explained in the following four parts.

a) Synthesis

In this (the third) chapter, one horizontal (E-W) component and the vertical (U-D) component are employed. We assume that the observed record, $F_0(t)$, of a large earthquake can be formulated approximately in the following Eq. (14) :

$$F_{0k}(t)=\sum_{i=1}^{N}\sum_{j=1}^{M}\alpha_{ki}\cdot g_{ki}(t)*h_{ij}(t)*E_{ki}\left(t-b_j-\frac{r_{ki}}{u_{ki}}\right) \quad (14)$$

b is the time lag from the first shock, subscript k indicates the k-th observation station, subscript i means the i-th grid point on the fault plane on which shocks are generated, subscript j means the j-th specific time when shocks are generated, N is the total number of grid points and M is the total number of specific times. Eq. (14) indicates that shocks are generated simultaneously at all the grid points on the fault plane at several fixed times. Other symbols are the same meanings as those in Eq. (1). Here some assumptions are introduced for simplification :

$$\alpha_{ki}=\alpha_k \quad (15)$$

$$E_{ki}(t)=E_k(t) \quad (16)$$

$$u_{ki}=\text{const.}=V_s \quad (17)$$

$$h_{ij}(t)=h_{ij} \quad (18)$$

Eqs. (15) and (16) show that a coefficient for the correction of radiation pattern, α, and Green's function, E, are constant, by disregarding the location of a grid point. We apply this synthesis to the S-waves which form the main parts of strong ground accelerograms. It is assumed that wave velocity is constant, as shown in Eq. (17). In Eq. (18), a function for the correction of the magnitude of a shock, $h(t)$, becomes a coefficient h. If we transpose a coefficient, α_k, from the right-hand side to the left-hand side in Eq. (14) and replace F_{0k}/α_k by F_{sk}, Eq. (19) is obtained :

$$F_{sk}(t)=\sum_{i=1}^{N}\sum_{j=1}^{M}h_{ij}\cdot g_{ki}(t)*E_k\left(t-b_j-\frac{r_{ki}}{V_s}\right) \quad (19)$$

$F_s(t)$ means the synthesized wave produced by the simuation. The ground motions of both a large earthquake and a small one must be recorded at all the stations. If we designate the locations and the times of the generation of shocks, we can calculate the values of g_i*E. $g_i(t)$ are the same as those represented in Eqs. (9)-(12), with the exception that the subscript becomes from e to i. Many synthesized waves are produced by giving various numerical values by trial and error to the constant coefficients, h_{ij}, which change spatiotemporally. These h_{ij} represent the spatiotemporal distribution for the generation of short-period body-waves. Because the calculation of inversion is invalid if we use the parts of the records which are influenced by the non-linear behavior of soft surface layers, we need to exclude the latter parts of the horizontal components in the records of a mainshock obtained on soft ground.

b) Criterion

In this section, the extent of the agreement of the synthesized waves with the obseved record is estimated. By frequency domain analysis, the following Eq. (20) is derived from Eqs. (14) and (19) :

$$\frac{F_{sk}(f)\ \ (\text{Synthesized wave})}{F_{0k}(f)\ \ (\text{Observed record})}=\frac{A(f)}{\alpha_k} \quad (20)$$

Where $A(f)$ is a function of frequency only and the average value on frequency components of a term $A(f)/\alpha_k$ must be adjusted so as to approach about unity (for example, 0.5~2.0). Eq. (20) is the judgement criterion in the frequency domain. In contrast, by time domain analysis, the next Eq. (21) is derived if we disregard the error of frequency components :

$$\frac{F_{sk}(t)\ \ (\text{Synthesized wave})}{F_{0k}(t)\ \ (\text{Observed record})}=\beta_k \quad (21)$$

Where β_k is a constant which depends on radiation pattern only and the average value on observation stations of β_k mnst be adjusted so as to approach about unity (for example, .0.5~2.0). Eq. (21) is the judgement criterion in the time domain. In this simulation, we select Eq. (21) which is the criterion in the time domain because there are many unstable factors in the frequency domain. β_k in Eq. (21) expresses the variation of amplitude ratio with azimuth.

c) Characteristics

The general natures of earthquakes are interpreted in the freuency domain, and the special property of

an individual earthquake is interpreted in the time domain. This is because a scaling law between earthquakes is discussed in the frequency domain, whereas a seismogram is easily combined with source parameters in the time domain. As a result, an inversion approach is generally done in the time domain. In contrast, because the attenuation of body-waves is remarkable in the short-period range, we may be able to make an inversion technique in the frequency domain on the basis of the difference in the degree of attenuation owing to frequency components, though, in this simulation, we do not use Eq. (20) which is the criterion in the frequency domain.

d) Simulation

Fig. 5 shows the fault zone and available observation stations for the Tokachi-oki earthquake. The small earthquake used here is shown in Table 1 and was used in the previous chapter. The assumed fault plane is expressed by the symbol * in Table 2 and was also used before. We need to remove the parts of the records affected by the non-linear behavior of soft surface layers. The available parts of accelerograms for the mainshock are summarized in Table 3. Subjectivity exists to some extent in the determination of the available parts.

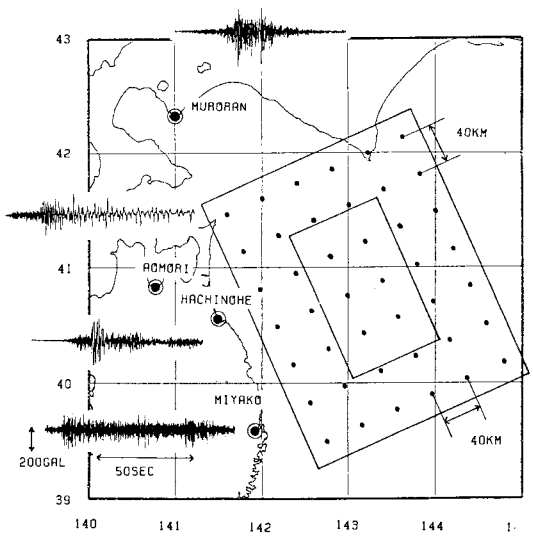

Fig. 5 The fault zone and available observation stations for the Tokachi-oki earthquake. The inner rectangle represents the fault zone inferred from aftershock distribution, and the outer rectangle represents the zone of the grid assumed in this calculation. 7 shocks are assumed to occur with 15 sec intervals at each grid point. The waveforms are E-W components at each observation station.

Table 3 The available parts of accelerograms for the mainshock.

	E-W	U-D
Muroran	90 sec	—
*Aomori	30 sec	105 sec
*Hachinohe	60 sec	90 sec
Miyako	105 sec	—

* shows the observation station affected by the non linear behavior of soft surface layers.
— means the record which can not be used for lack of a record for a small earthquake.

First, we appoint the locations and the times of the occurrence of shocks. We determine the zone of a grid as shown in Fig. 5 so as to cover widely the rectangular fault zone which was roughly estimated on the basis of aftershock distribution. 42 (7×6) point sources are arranged on the grids spaced at 40km, and 7 shocks are assumed to occur with 15 sec intervals at each grid point. 90 sec ($(7-1)\times15=90$) are assumed as the process time of the total rupture, which must be taken up enough long. The ratio of the magnitude of the amplitude of the seismogram for each shock to that for Green's function is estimated as the value closest to one of 0, 0.5, 1.0, 2.0, 3.0 and 4.0. These numerical values are assumed as a matter of convinience. Besides, S-wave velocity is fixed at $V_s=4.0$ km/sec and S-wave quality factor is fixed at $Q_{ss}=Q_{si}=500$, which are the same values as the calculation in the previous chapter.

In Eq. (19), the horiontal motions of the mainshock are synthesized from Green's functions for horizontal motions and the vertical motions are synthesized from Green's functions for vertical motions without correcting radiation pattern. Therefore, synthesized waves F_{st} include the error due to source directivity.

In the following part, the procedure for judgment is explained, that is, the contents of Eq. (21) are embodied. It is to evaluate the extent of the agreement of a synthesized wave with the observed record, each time a synthesized wave is shifted at a constant interval, ΔSH, along the time axis and to determine the best correspondence that minimizes the error between the two waves. This technique is introduced in

order to roughly match the shape of the envelop of a synthesized waves with that of the observed record in the time domain.

(i) First, we do the following step at each observation station. The absolute time of horizontal motion $[H]$ corresponds to that of vertical motion $[V]$. We divide each component (E-W and U-D) of the observed record into consecutive ΔT intervals and evaluate the sum of the absolute values of amplitude for each interval. We define them as $RT_{id}^{[H]}$ ($id=1\sim k_H$, k_H is the total number of intervals) for horizontal motion and as $RT_{id}^{[V]}$ ($id=1\sim k_V$, k_V is the total number of intervals) for vertical motion. After that, the values are normalized by the following Eqs. (22) and (23) because all the parts at all stations for each interval of ΔT must be estimated with equal weight:

$$\frac{RT_{id}^{[H]}}{\sum_{id=1}^{kH} RT_{id}^{[H]}} \cdot k_H \cdot \Delta T = RU_{id}^{[H]} \quad \cdots\cdots (22)$$

$$\frac{RT_{id}^{[V]}}{\sum_{id=1}^{kV} RT_{id}^{[V]}} \cdot k_V \cdot \Delta T = RU_{id}^{[V]} \quad \cdots\cdots (23)$$

(ii) On the othre hand, we pich out the $k_H \cdot \Delta T$ interval for horizontal motion and the $k_V \cdot \Delta T$ for vertical motion from the beginning of a synthesized wave, which has a longer duration than an observed record. We divide each component of the synthesized wave into consecutive ΔT intervals and evaluate the sum of the absolute values of amplitude for each interval. We define them as $ST_{id}^{[H]}(jd=1)(id=1\sim k_H)$ and as $ST_{id}^{[V]}(jd=1)(id=1\sim k_V)$. After that, the values are normalized by the following Eqs. (24) and (25):

$$\frac{ST_{id}^{[H]}(jd=1)}{\sum_{id=1}^{kH} ST_{id}^{[H]}(jd=1)} \cdot k_H \cdot \Delta T = SU_{id}^{[H]}(jd=1) \quad \cdots\cdots (24)$$

$$\frac{ST_{id}^{[V]}(jd=1)}{\sum_{id=1}^{kV} ST_{id}^{[V]}(jd=1)} \cdot k_V \cdot \Delta T = SU_{id}^{[V]}(jd=1) \quad \cdots\cdots (25)$$

Next, we pick out the $k_H \cdot \Delta T$ interval and the $k_V \cdot \Delta T$ interval from the ΔSH after the begining and calculate the values of $SU_{id}^{[H]}(jd=2)$ and $SU_{id}^{[V]}(jd=2)$ in the same procedure. Further, we pick out the $k_H \cdot \Delta T$ and $k_V \cdot \Delta T$ intervals from $2 \cdot \Delta SH$ after the beginning and obtain the values of $SU_{id}^{[H]}(jd=3)$ and $SU_{id}^{[V]}(jd=3)$. This procedure is repeated L times ($jd=1\sim L$) until the synthesized wave comes to an end.

(iii) We vary jd from 1 to L in the following Eq. (26):

$$Z_K = \sum_{id=1}^{kH} \left| RU_{id}^{[H]} - SU_{id}^{[H]}(jd) \right| + \sum_{id=1}^{kV} \left| RU_{id}^{[V]} - SU_{id}^{[V]}(jd) \right| \quad \cdots\cdots (26)$$

We calculate the minimum value of the function, Z_k, and define it as TO_k at station K. Since the absolute time is unknown at each station, we calculate the sum, TO, of the values of TO_k for all the stations. The combination of the coefficients, h_{ij}, that minimizes the value of TO represents the most suitable spatiotemporal distribution for the generation of short-period body-waves. Here, ΔT and ΔSH are fixed at 15 sec and 5 sec, respectively. Then, the values of k_H, k_V and L are automatically determined at each observation station.

(iv) In addition, we compute the values of β_k in Eq. (21) at all the stations by using the following Eqs. (27) and (28):

$$\beta_k^{[H]} = \frac{\sum_t |F_{sk}^{[H]}(t)|}{\sum_t |F_{0k}^{[H]}(t)|} \quad \cdots\cdots (27)$$

$$\beta_k^{[V]} = \frac{\sum_t |F_{sk}^{[V]}(t)|}{\sum_t |F_{0k}^{[V]}(t)|} \quad \cdots\cdots (28)$$

(4) Results

We observe the case that best satisfies the judgement criterion. However, the uniqueness and accuracy of this case can not be guaranteed because the solution can not be determined uniquely by this technique and the total number of simulations is not sufficient.

First, Fig. 6 shows a part of the comparisons of the synthesized waves with the observed records. The amplitude of synthesized waves is normarized so that both $\beta_k^{[H]}$ and $\beta_k^{[V]}$ may become unity (1.0). The agreement between the synthesized waves and the observed records is satisfactory in the shape of the envelop of waveform. The synthesized wave of the E-W component at Hachinohe station becomes improved enough, when compared with the result in Fig. 4. Next, Fig. 7 represents the spatiotemporal distribution for the generation of short-period body-waves. Fig. 8 shows the spatial distribution of generation. The amount given at each location is an accumulation for the total process time. It is inferred from these results that the Tokachi-oki earthquake is a very complicated source rupture process over a wide area. In addition, the values of $\beta_k^{[H]}$ and $\beta_k^{[V]}$ are summarized in Table 4. The amplitude ratio varies with azimuth by a factor 3 or 4.

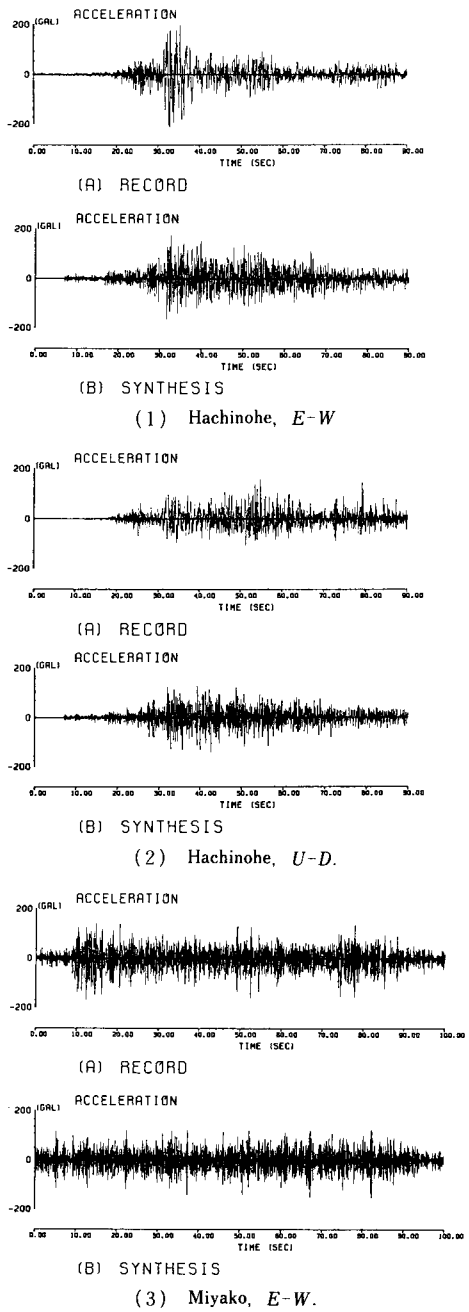

Fig. 6 A part of the comparisons at each observation station in the Tokachi-oke earthquake.

(5) Discussion

First, we calculate the sum of the coefficients, h_{ij}. The value is 103.5. It is interpreted that this value represents the ratio of the amount of generation of short-period body-waves between a large earthquake and a small one. According to the study of the source spectrum for body-waves, the source spectrum reaches an upper limit regardless of the increase of the magnitude of an earthquake. It is inferred from the result of our study that at least the ratio between the two earthquakes of the amount of short-period body-waves generated in the source is very large.

In this earthquake, a distinct rupture front can not be recognized. The direction of the main-fault propagation is compatible with the results of the study by Kanamori[5], which is based upon long-period surface-waves. However, it is implied that the source rupture process is very complex and that the stress increases gradually on the fault plane.

Next, the coefficient, β_k, expresses the relative ratio of the amplitude of the accelerogram for the large

Table 4 The variatios, with azimuth of the amplitude ratio, β_k, of synthesized waves to observed records.

	E-W	U-D
Muroran	0.83	—
Aomori	1.47	0.76
Hachinohe	1.37	1.01
Miyako	3.43	—

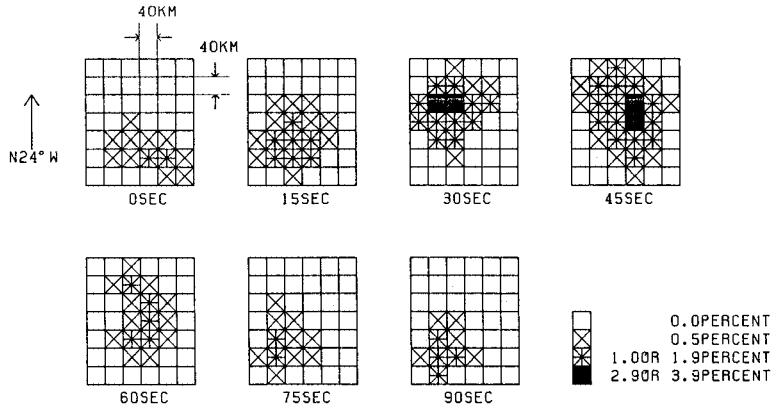

Fig. 7 The spatiotemporal distribution for the generation of short-period body-waves. Symbols represent the ranking of the ratio of the amount generated at each location and time for the total generation. The location of grids is shown in Fig. 5.

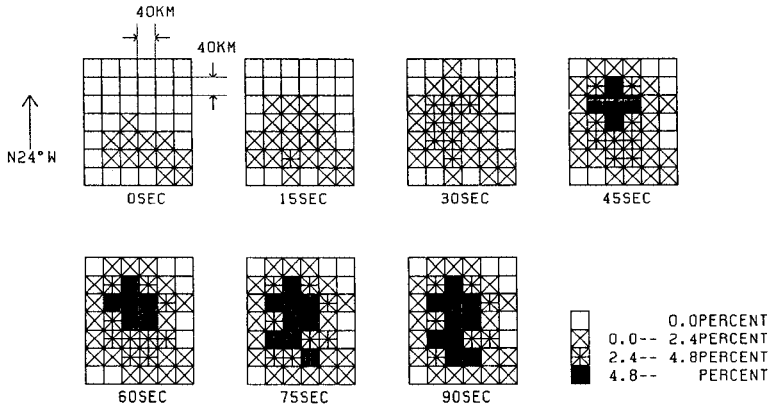

Fig. 8 The spatial distribution for the generation of short-period body-waves. The amount given at each location is an accumulation for the total process time. Symbols are the same meaning as those in Fig. 7.

earthquake to that of the small one. It is noticeable that β_k varies with azimuth by a factor of 3 or 4. Though the factor of source directivity has been disregarded up to now in short-period range in earthquake engineering, this result implies that traditional ways of thinking may be inadequate. Recently, Boatwright and Boore[12] indicated that the source directivity caused a variation of a factor of 10 in peak acceleration.

4. CONCLUSION

In this study, we intend to clarify the complexity of large earthquakes by considering the ground motions of short-period range. First, a revised approach[1] has been applied to three large earthquakes. As a result, it has been confirmed that this approach can be applicable in all cases to some degree. However, it is implied that a larger earthquake is more complicated. Next, we have developed an inversion method applicable to short-period range and have applied the method to the Tokachi-oki earthquake. It has been inferred from the obtained results that this earthquake has a complicated source rupture process and has source directivity even in short-period range. It is thought that this inversion method is exceedingly effective.

ACKNOWLEDGMENTS

The Department of Structure of the Port and Harbour Research Institute of Japanese Ministry of Transport kindly gave us permission to study the accelerograms used in this study. We have been indebted to Dr. Ryosuke Inoue, Associate Professor Yozo Fujino, Dr. Toshiyuki Katada and Dr. Takashi Miyatake for helpful advice and encouragement.

REFERENCES

1) Iida, M. and Hakuno, M. : The synthesis of the acceleration wave in a great earthquake by small earthquake records, Proc. Japan Soc. Civil Eng., 329, pp. 57～68, 1983 (in Japanese).
2) Hartzell, S. H. : Earthquake aftershocks as Green's functions, Geophys. Res. Letters, Vol. 5, pp. 1～4, 1978.
3) Seno, T., Shimazaki, K., Somerville, P., Sudo, K., and Eguchi, T. : Rupture process of the Miyagi-oki, Japan, earthquake of June 12, 1978, Phys. Earth Planet. Inter., 23, pp. 39～61, 1980.
4) Shimazaki, K : Nemuro-oki earthquake of June 17, 1973 : a lithospheric rebound at the upper half of the interface, Phys. Earth Planet. Inter., 9, pp. 314～327, 1975.
5) Kanamori, H. : Focal mechanism of the Tokachi-oki earthquake of May 16, 1968 : contortion of the lithosphere at a junction of two trenches, Tectonophysics, 12, pp. 1～13, 1971.
6) Burdick, J. L. and Mellma, G. R. : Inversion of body waves from the Borrego Mountain earthquake to the source mechanism, Bull. Seism. Soc. Am., Vol. 66, pp. 1485～1499, 1976.
7) Langston, C. A. : A body wave inversion of the Koyna, India, earthquake of December 10, 1967, and some implications for body wave focal mechanism, J. Geophys. Res., Vol. 81, pp. 2517～2529, 1976.
8) Boatwright, J. : Preliminary body-wave analysis of the St. Elias, Alaska, earthquake of February 28, 1979, Bull. Seism. Soc. Am., Vol. 70, pp. 419～436, 1980.
9) Kikuchi, M. and Kanamori, H. : Inversion of complex body waves, Bull, Seism. Soc. Am., Vol. 72, pp. 491～506, 1982.
10) Trifunac, M. D. and Brune, J. N. : Complexity of energy release during the Imperial Valley, California, earthquake of 1940, Bull. Seism. Soc. Am., Vol. 60, pp. 137～160, 1970.
11) Fujino, Y., Hamazaki, T., and Inoue, R. : Identification of multiple rupture process of 1979 Imperial Valley earthquake by near-field accelerograms, Proc. 6th Japan Earthq. Eng. Symp., pp. 97～104, 1982.
12) Boatwright, J. and Boore, D.M. : Analysis of the ground accelerations radiated by the 1980 Livermore Valley earthquake for directivity and dynamic source characteristics, Bull. Seism. Soc. Am., Vol. 72, pp. 1843～1865, 1982.

(Recieved December 23 1983)